

Effect of extra electrons on the exchange and magnetic anisotropy in the anionic single-molecule magnet Mn_{12}

Kyungwha Park^{1,2*} and Mark R. Pederson^{1†}

¹*Center for Computational Materials Science, Code 6390,
Naval Research Laboratory, Washington DC 20375*

²*Department of Physics, Georgetown University, Washington DC 20057*

(Dated: November 15, 2018)

Abstract

To understand the effect of molecular environment on the electronic and magnetic properties of the single-molecule magnet (SMM) Mn_{12} , we explore two possible means for adding extra electrons to molecule. We explore both substitution of Mn ions by Fe ions and the inclusion of neighboring electronic donors. For both possibilities we calculate, within density-functional theory, the electronic structure, the total ground-state spin and ordering, the magnetic anisotropy barrier, the transverse magnetic anisotropy parameter E which is responsible for some measured tunneling, and the tilting angle of the easy axis from the z axis. Our calculations show that the total spin increases with increasing number of extra electrons except for the case of Mn_8Fe_4 where the resulting ground state has a low spin. The calculated energy gaps between the unoccupied and the occupied orbitals exhibit no clear trend as a function of number of extra electrons. The calculated magnetic anisotropy barrier decreases with increasing number of extra electrons and can be directly chased to a quenching of Jahn-Teller distortions at the sites where the additional electrons are localized. The values of E and the easy-axis tilting angles for the geometries with one- and two-extra electrons are significantly larger than those induced by solvent disorder.

PACS numbers: 75.50.Xx, 71.15.Mb, 75.30.Gw, 75.30.Et

I. INTRODUCTION

There has been a great demand for high-density magnetic recording media that can store a bit of information on a nanoscale magnetic particle or molecule. Periodic arrays of high-spin molecules (each molecule having a volume of a few nm³) could be potentially useful for this purpose. These high-spin molecules consist of several transition metal ions which are strongly coupled to each other and are surrounded by various ligands. The intermolecular interactions are quite weak and each molecule has a large energy barrier to magnetization reversal (i.e. magnetic anisotropy barrier). This leads to a behavior analogous to that of single-domain magnetic nanoparticles in an external magnetic field at low temperatures. Because of their behavior, the molecules are referred to as single-molecule magnets (SMMs). Although typical SMMs are paramagnetic, they exhibited magnetic hysteresis loops at low temperatures^{1,2} similar to that of ferromagnets at room temperatures. This is because their magnetic moments are frozen so that they relax on scales that are slow compared to the measurement time. The striking observation on SMMs was that they revealed quantum tunneling of magnetic moment³ through the magnetic anisotropy barrier (MAB), which were confirmed by various experiments including temperature independent magnetic hysteresis loops^{1,2} and temperature independent relaxation time of magnetic moment⁴.

Among hundreds of synthesized SMMs, [Mn₁₂O₁₂(CH₃COO)₁₆(H₂O)₄]·2(CH₃COOH)·4(H₂O) (hereafter Mn₁₂),⁵ has been the most extensively studied experimentally and theoretically. The strong interest is due to Mn₁₂ being the first synthesized SMM and to the fact that to date it provides the largest MAB of 65 K.^{6,7,8} The MAB is directly related to the temperature below which magnetic moments are frozen. A general spin Hamiltonian for a SMM is, to lowest order,

$$\mathcal{H}_0 = DS_z^2 + E(S_x^2 - S_y^2) + g\mu_B \vec{B} \cdot \vec{S} \quad (1)$$

where S_z is the spin operator projected onto the z axis which is the magnetic easy axis, D and E are the uniaxial and transverse second-order magnetic anisotropy parameters caused by spin-orbit coupling. The last term is the Zeeman interaction. In \mathcal{H}_0 , the odd-order terms in S vanish due to time reversal symmetry at zero field. High-field, high-frequency electron paramagnetic resonance (EPR) experiments on the SMM Mn₁₂ provided $D = -0.55$ K.^{6,7,8} Considering the S_4 symmetry of a Mn₁₂ molecule (without solvent molecules), we know that $E = 0$. Quantum tunneling of magnetic moment is then allowed for pairs of states that

satisfy a certain selection rule: The two states must have S_z -eigenvalues differing by integer multiples of 4. However, tunneling between states which violate this selection rule are clearly observed in magnetic tunneling measurements.^{1,2} To resolve this puzzle, three different theories have been proposed.^{9,10,11,12} Chudnovsky and Garanin⁹ proposed any dislocations in single crystals could produce a broad continuous distribution in E . Detailed x-ray diffraction studies by Cornia *et al.*¹⁰ suggested that disorder caused by acetic-acid (CH_3COOH) solvent molecules could break the S_4 symmetry and provide nonzero locally varying E values. Magnetic quantum tunneling¹³ and high-field, high-frequency EPR experiments¹⁴ showed that their experimental data are not in quantitative accord with the Cornia *et al.*'s model¹⁰. Recent density-functional theory (DFT) calculations¹¹ showed that for quantitative comparison with experiment, geometry relaxation must be considered. Pederson *et al.* suggested that coupling between the magnetic and vibrational degrees of freedom leads to the standard fourth-order form of the anisotropy Hamiltonian for *isotopically pure samples*.¹² However, they showed that for isotopically impure samples¹⁵ there are two different vibrational effects that cause symmetry and a coupling between M and $M \pm 2$ states and that the symmetry breaking would be random assuming the isotopic substitution was.

Very recent experiments on the SMM $[\text{Mn}_{12}\text{O}_{12}(\text{O}_2\text{CCH}_2\text{Br})_{16}(\text{H}_2\text{O})_4] \cdot 8\text{CH}_2\text{Cl}_2$ (hereafter $\text{Mn}_{12}\text{-BrAc}$) showed that there is a broad distribution in internal transverse fields (7.3° for a standard deviation).¹⁶ For this case the molecules of crystallization CH_2Cl_2 have higher symmetry and probably do not break the intrinsic S_4 symmetry in contrast to the acetic acid solvent molecules in the standard Mn_{12} crystal. It has been suggested that the distribution in internal transverse fields could arise from a distribution in the magnetic easy axes of individual molecules.^{16,17} But the origin of the distribution in the magnetic easy axes remains unknown. In this regard, we consider, within DFT, the possibility that extra electrons when accepted by Mn_{12} molecules, will exhibit a disorder- or defect-induced behavior that is observed in the experimental samples.

The SMM Mn_{12} has four Mn^{4+} ions at the corners of the inner cubane and eight Mn^{3+} ions in the outer crown (Fig. 1). The magnetic moments of the eight Mn^{3+} ions ($S = 2$) were observed to be antiparallel to those of the four Mn^{4+} ions ($S = 3/2$), which leads to a total ground-state spin of $S = 10$.¹⁸ The observed magnetic structure and the MAB for the ground state of the Mn_{12} has been calculated in recent DFT calculations.¹⁹ The exchange interactions between metal ions have also been calculated²⁰ within DFT. Both the MAB and

exchange interactions are in very good agreement with experiments.²¹ Despite an increasing number of synthesized SMMs, it is not well understood what types of variations in the molecular environment influence the magnetic structure, the intramolecular exchange interactions, and the MAB of the molecule. Hendrickson’s and Christou’s groups synthesized two types of anionic SMM Mn_{12} and performed magnetic measurements on them.^{22,23,24} One type is gleaned by substitution of four Mn ions by four Fe ions in the ordinary Mn_{12} structure, $[\text{Mn}_8\text{Fe}_4\text{O}_{12}(\text{CH}_3\text{COO})_{16}(\text{H}_2\text{O})_4]$ (hereafter experimental Mn_8Fe_4).²² The other is synthesized by adding one or two PPh_4 molecules ($\text{Ph}\equiv\text{C}_6\text{H}_5$) to a Mn_{12} molecule containing different ligands from the ordinary Mn_{12} , $(\text{PPh}_4)[\text{Mn}_{12}\text{O}_{12}(\text{O}_2\text{CCH}_2\text{CH}_3)_{16}(\text{H}_2\text{O})_4]$ (hereafter $(\text{PPh}_4)\text{Mn}_{12}$) and $(\text{PPh}_4)_2[\text{Mn}_{12}\text{O}_{12}(\text{O}_2\text{CCHCl}_2)_{16}(\text{H}_2\text{O})_4]$ (hereafter $(\text{PPh}_4)_2\text{Mn}_{12}$). A PPh_4 molecule has one unpaired electron with A_1 symmetry and may be thought of as a molecular alkali.^{23,24} Magnetic measurements on both types revealed that their total spins, magnetic susceptibilities, and MABs significantly changed with the number of extra electrons but that the two types are partially but not entirely homologous.^{22,23,24} As far as we know, no theoretical studies on these interesting results have been reported.

As implied earlier, our motivation is twofold. One is to understand how the microenvironment within a Mn_{12} molecule controls its magnetic properties. The other is to view extra electrons as disorder or defects in the Mn_{12} structure and to understand their effects on S_4 symmetry-breaking terms in the spin Hamiltonian Eq. (1). Motivated by the experiments described in the previous paragraph, we employ DFT to investigate two categories of environments where extra electrons can be transferred to metal ions in a single Mn_{12} molecule: (i) substitution of Fe for Mn and (ii) addition of electronic donors such as K to the molecule. In the first case, since an Fe atom has one more electron than a Mn atom, replacing Mn by Fe will play the role of donating one extra electron to the ordinary Mn_{12} structure. In the second case, since a PPh_4 molecule has one unpaired electron, addition of PPh_4 molecules to a Mn_{12} molecule is equivalent to adding single-electron donors to the Mn_{12} molecule. In our calculations, K atoms were used instead of large PPh_4 molecules because a K atom also has one unpaired electron and it reduces computational cost. In the sense that there are extra electrons in the ordinary Mn_{12} structure, we call the SMMs under the new environment the anionic SMM Mn_{12} . For both categories, we consider one-, two-, and four- extra electrons donated to the Mn_{12} molecule. For each anionic state, we calculate the electronic structure, the total magnetic moment, and the magnetic anisotropy parameters, using DFT. We

find that Fe substitution provides similar results (not exactly same) to K addition and that some microenvironments drastically alter the magnetic structure. In Sec. II, we describe our detailed model and method. In Secs. III and IV, we separately present DFT calculations on the electronic and magnetic properties for Fe substituted and K added geometries. In Secs. V and VI, we present our discussion and conclusion.

II. MODEL AND METHOD

Our DFT calculations²⁵ are performed with spin-polarized all-electron Gaussian-orbital-based Naval Research Laboratory Molecular Orbital Library (NRLMOL)²⁶. Here the Perdew-Burke-Ernzerhof (PBE) generalized-gradient approximation (GGA) is used for the exchange-correlation potential.²⁷ For all atoms full basis sets are used with a fine numerical integration mesh unless otherwise specified.²⁸ Prior to geometry relaxation, an initial spin configuration must be assigned with an initial total moment that can either be fixed or optimized. An optimized geometry is obtained when forces on all atoms become small. To find the ground-state spin configuration, different spin configurations with different total magnetic moments are considered. The second-order magnetic anisotropy parameters are calculated for an optimized geometry using the technique described in Ref.[19].

As initial geometries for the two types of environmental changes, we start with a simplified form of a Mn_{12} molecule with S_4 symmetry, $[\text{Mn}_{12}\text{O}_{12}(\text{HCOO})_{16}(\text{H}_2\text{O})_4]$. Here 16 acetates (CH_3COO) in the experimental Mn_{12} were replaced by 16 formates (HCOO) (refer to Fig. 1). Earlier calculations on the Mn_{12} molecule showed that the energy gap between the majority HOMO (highest occupied molecular orbital) and the minority (majority) LUMO (lowest unoccupied molecular orbital) is about 0.804 eV (0.438 eV).¹⁹ The calculated majority HOMO-LUMO energy gap agreed with the result of the recent electrical resistivity measurement, 0.37 ± 0.05 eV.²⁹ The total ground-state moment was calculated to be $20\mu_B$, which agreed with experiment. The calculated second-order MAB was 54 K in zero field, which did not change much with our simplification of the molecule. Hereafter, unless specified, Fe substitution and K addition will be carried out in the above simplified form of a Mn_{12} molecule.

For the optimized geometry of the Mn_{12} molecule, the first four unoccupied majority orbitals directly above the Fermi level are close to each other in energy but well separated from

the rest of unoccupied orbitals. The four orbitals contain the LUMO, an orbital 0.008 eV above the LUMO, and doubly degenerate orbitals 0.012 eV above the LUMO. The fifth orbital is 0.212 eV above the LUMO. Because the third and fourth orbitals are degenerate, the case of three extra electrons is not considered in our DFT calculations. But our prediction of the case based on symmetry will be provided in Sec. V. We first examine whether there are any favorable sites for the extra electrons in the Mn_{12} geometry when four Fe ions are substituted in a S_4 symmetric fashion. Then when four-, two-, and one-extra electrons are accepted in a Mn_{12} molecule under each type of environment, we calculate HOMO-LUMO energy gaps, the total ground-state moment, and the ground-state spin configuration. In various ways, we examine whether the extra electrons are well localized at some of the Mn sites. Using the optimized geometry with the ground-state spin configuration, we calculate the MAB, the transverse magnetic anisotropy parameter E , and the magnetic easy axis. When experimental data are available, comparison between calculations and experiment are discussed.

III. DFT CALCULATIONS: IRON SUBSTITUTION

The S_4 symmetry and the geometry of the Mn_{12} provide three symmetrically inequivalent Mn sites such as one inner cubane site (α) and two inequivalent outer crown sites (β and δ) shown in Fig. 1. To locate an energetically favorable site for accepting extra electrons, we consider the three S_4 symmetric configurations in which four Mn ions are replaced by Fe ions at the three inequivalent sites, $[\text{Mn}_8\text{Fe}_4\text{O}_{12}(\text{HCOO})_{16}(\text{H}_2\text{O})_4]$ (hereafter Mn_8Fe_4). When four Mn ions at the sites α are replaced, the configuration is called the geometry α . A similar definition is applied to the geometries β and δ . The geometry δ is shown in Fig. 1. The energies of the three tetra-Fe substituted geometries are self-consistently calculated with the total magnetic moment fixed and with the spin configuration illustrated in Fig. 2(a) (only the direction of each Mn moment is assigned such as spin up or down). Then we calculate HOMO-LUMO energy gaps and check whether Fermi filling is satisfied for the three geometries with two different fixed moments ($24\mu_B$ and $22\mu_B$). If there exist appreciable HOMO-LUMO energy gaps and the calculated orbitals abide by the Fermi filling, then the system is regarded as being magnetically stable. As summarized in Table I, the energy is the lowest among the six possible configurations when four Fe ions occupy the site

δ given the total moment of $24\mu_B$. Local moments around the Fe sites for the geometries β and δ with the total moment of $24\mu_B$, are found to be $3.94\mu_B$ and $3.95\mu_B$ within a sphere with 2.23 Bohr radius (Table I). These local moments are definitely larger than those at the other outer Mn sites, 3.59 - $3.64\mu_B$, for the Mn_8Fe_4 geometries or those at the outer Mn sites, 3.55 - $3.62\mu_B$, for the Mn_{12} geometry. But the local moment at the Fe site for the geometry α is greatly reduced to $-1.55\mu_B$. This is because the initial spin configuration [Fig. 2(a)] does not permit the extra electrons to be localized in the cubane. The same trend appears for the local moments of the geometry with the total moment of $22\mu_B$. Our finding of the δ to be energetically favored is also evidenced in the site calculated density of states projected onto the three inequivalent Mn($3d$) orbitals for the Mn_{12} geometry. As shown in Fig. 3, the preferred site δ has the largest majority density of states directly above the Fermi level. This finding is also corroborated by x-ray crystallographic data on the experimental Mn_8Fe_4 .²² Henceforth we consider only cases where Fe is substituted for Mn at the site δ .

A. Four Fe substitution: Mn_8Fe_4

Our initial study showed that the Mn_8Fe_4 geometry with the total moment of $24\mu_B$ has lower energy than that with the total moment of $22\mu_B$. The measurement on the experimental Mn_8Fe_4 , however, revealed that the static magnetic susceptibility for this SMM has a completely different temperature dependence from that of the Mn_{12} ($S = 10$), which led to the ground state of $S = 2$ for the former.²² So following the method discussed in Refs. 20,33 we examine several low-spin states to search for the ground state. In this study, we consider collinear spin states only. For a particular total moment, there are numerous spin configurations. We thus select a few spin configurations to test, considering that the exchange interactions between the Mn ions and Fe ions through the oxygen ligands (i.e. superexchange interactions)³⁰ prefer antiferromagnetic coupling. We calculate the energies for six selected spin configurations with $M_s = 2$ and for five chosen configurations with $M_s = 4$ where M_s is an eigenvalue of S_z . Some of the configurations and their calculated energies are specified in Table II and Fig. 2(b). Our calculations show that the ground state may have the total moment of $8\mu_B$ ($M_s = 4$) with the spin configuration indicated in the sixth row of Table II and Fig. 2(b). Apparently this does not agree with the original experiment²² but a very recent experiment on $[\text{Mn}_8\text{Fe}_4\text{O}_{12}(\text{O}_2\text{CCH}_2\text{Cl})_{16}(\text{H}_2\text{O})_4]$ suggested

that the ground state may have a spin of $S = 4$.³¹ Notice that the CH_2Cl molecules in this compound take up the position of the CH_3 molecules in the experimental Mn_8Fe_4 compound. In our calculations, we terminated the carboxyl groups with hydrogen atoms rather than CH_3 radicals in the Mn_8Fe_4 geometry. Other possible reasons, such as a highly correlated many-spin wavefunction, for this discrepancy will be discussed later in this section and in Sec. V.

We discuss the electronic and magnetic properties for the lowest-energy structure of the Mn_8Fe_4 which has the total moment of $8\mu_B$ and the spin configuration specified in Table II and Fig. 2(b). The energy gap between the majority HOMO and the minority (majority) LUMO is about 0.664 eV (0.247 eV). So the ground state is magnetically stable. The local moments of the inner Mn (the site α), outer Mn (the site β), and outer Fe ions (the site δ) are found to be $2.61 \mu_B$, $3.48 \mu_B$, and $-4.16 \mu_B$, respectively, within a sphere of 2.23 Bohr radius. Since the wave functions of Fe and Mn ions overlap with those of other neighboring atoms, the sphere around each ion does not capture a full moment. When we compare the local moments with those for the Mn_{12} shown in the second column of Table I, we find that only the local moment of the outer Fe ion substantially increases. Based on the calculations, we speculate that the inner and outer Mn ions and outer Fe ions correspond to Mn^{4+} ($S = 3/2$), Mn^{3+} ($S = 2$), and Fe^{3+} ($S = 5/2$), respectively. This gives the ground-state spin of $S = 4 \times 3/2 + 4 \times 2 - 4 \times 5/2 = 4$. The total MAB is calculated to be 33 K, which is approximately 60% of the MAB for the ordinary Mn_{12} , 54 K (Table III). Since the ground state has S_4 symmetry, there is no transverse magnetic anisotropy, $E = 0$. Using the method described in Refs.11,32, we calculate the projected MABs and the local easy axes of the three different metal sites. As shown in Table IV (the third column), the local magnetic anisotropy of the Mn ions at the sites β mainly contributes to the total MAB. In contrast to the Mn_{12} geometry, the Fe ions at the sites δ have little contributions to the total MAB. This is supported by the calculated local easy axes of the three sites. The local easy axis at the site α is nearly in the x - y plane. The site δ has a local easy axis 65.8° away from the z axis (global easy axis), while the site β has a local easy axis only 8.5° away from the z axis. As illustrated at the bottom of Fig. 1, an Fe^{3+} ion in a distorted octahedral environment has exactly half-occupied e_g and t_{2g} $3d$ orbitals, which leads to an absence of Jahn-Teller distortion as would be the case for a Mn^{4+} ion and a Mn^{2+} ion. Thus the total MAB arises from single-ion anisotropy of the four Mn ions at the sites β only.

Since the Mn_8Fe_4 geometry has a very different ground state from the Mn_{12} , it is worthwhile to explore the exchange interactions between metal ions within a Mn_8Fe_4 molecule. For this purpose, we consider collinear spin configurations with $M_s = 5, 6, 7$, and 8 in addition to the previously discussed several configurations with $M_s = 2$, $M_s = 4$ and $M_s = 12$ (Table II). The technique to calculate the exchange interactions using DFT was described elsewhere.^{20,33,34} As illustrated in Fig. 2(b), there are six different exchange coupling constants within a Mn_8Fe_4 molecule such as J_1 , J_2 , J_3 , J'_3 , J_4 , and J'_4 . Here J_3 (J_4) is slightly different from J'_3 (J'_4) because of a small difference in the bond lengths. To compare with other references, we take an average of the two slightly different exchange constants. The spin Hamiltonian considered for the calculation of the exchange constants is

$$\begin{aligned} \mathcal{H}_{\text{ex}} = & E_0 + J_1 \sum_{i=1}^4 S_i S_{i+4} + J_2 \left\{ \sum_{i=1}^3 (S_i + S_{i+1}) S_{i+8} + (S_4 + S_1) S_{12} \right\} + J_3 \left\{ \sum_{i=1}^3 S_i S_{i+1} + S_4 S_1 \right\} \\ & + J'_3 \sum_{i=1}^2 S_i S_{i+2} + J_4 \left\{ S_5 S_{12} + \sum_{i=6}^8 S_i S_{i+3} \right\} + J'_4 \sum_{i=5}^8 S_i S_{i+4} \end{aligned} \quad (2)$$

where E_0 is the background energy. All spins are of Ising type and they are numbered as illustrated in Fig. 2(b). From the DFT-calculated energies of the fourteen configurations (Table II), we extract the seven unknown parameters, E_0 , J_1 , J_2 , J_3 , J'_3 , J_4 , and J'_4 using a least-square-fit method. Table V exhibits our calculated exchange constants in comparison with experimentally estimated values and the exchange constants for the Mn_{12} geometry.³⁵ In contrast to the Mn_{12} geometry, the Mn_8Fe_4 geometry has strong antiferromagnetic interactions between the outer Mn and Fe ions (J_4 between the sites β and δ), which are comparable to the interactions between the inner Mn and outer Mn ions (J_1 between the sites α and β and J_2 between the sites α and δ). This tendency was also observed in the experimental estimates. For a quantitative comparison of the calculated values with experiment, more refined experiments which are sensitive to the exchange constants are required. With the calculated exchange constants, one can construct the isotropic Heisenberg Hamiltonian. The true ground state is obtained by exact diagonalization of the Heisenberg Hamiltonian.^{20,33,34} The size of the Hilbert space to diagonalize is 207 360 000. We do not further pursue the ground state of the system by exact diagonalization of the large Hamiltonian matrix. The MAB varies with spin configurations from 16 K to 33 K as shown in the last column of Table II. This large variation was not found for the SMMs Mn_{12} and Mn_4 monomer.^{20,34} We speculate that the reason may be related to the fact that for the Mn_8Fe_4 the considered

spin configurations have energies of the same order of single-electron excitations (Table III).

B. Double and single Fe substitutions: $\text{Mn}_{10}\text{Fe}_2$ and Mn_{11}Fe

There are two inequivalent possible ways to replace two Mn ions at the sites δ by Fe ions. One way is to place two Fe ions in a twofold symmetric fashion ("trans"). The other is to place Fe ions in a unsymmetrized fashion ("cis"). With the spin configuration shown in Fig. 2(a), we obtain an optimized total moment of $22\mu_B$ for the *trans* and *cis* geometries. The experiment on the SMM $(\text{PPh}_4)_2\text{Mn}_{12}$ suggested that the ground-state may have a total spin of $S = 10$.²⁴ So we consider several spin configurations with $M_s = 10$ (*trans*) that might have lower energies than the energy of the configuration with $M_s = 11$. A good candidate is the configuration obtained by flipping only two spins coupled by J_1 from the configuration with $M_s = 11$ (Refer to Figs. 2(a) and (b)). We find that the configuration with $M_s = 10$ has an energy 0.014 eV above the energy of the considered configuration with $M_s = 11$ (Table VI). Thus, the ground state has a total moment of $22\mu_B$. We calculate the electronic and magnetic properties for the ground state. For the *trans* geometry, the energy gap between the majority HOMO and the minority (majority) LUMO is 0.075 eV (0.432 eV). The value of E is 0.045 K and the MAB is 31 K (Table III). The calculated projected anisotropy on the sites α , β , and δ implies that only the site β contributes to the total MAB (Table IV). For the *cis* geometry, the energy gap between the majority HOMO and the minority (majority) LUMO is 0.030 eV (0.427 eV). The value of E is 0.020 K and the MAB is 33 K. The magnetic easy axis is tilted by 19° from the z axis (Table III). Notice that the value of E for the *cis* geometry does not cancel out. This contrasts with a negligibly small E value calculated for the $n = 2$ *cis* configuration in a Mn_{12} molecule with disordered solvent.^{10,11} The MAB for the *cis* geometry agrees with that for the *trans* within numerical uncertainty. This barrier is significantly reduced compared to that for Mn_{12} due to an absence of the Jahn-Teller distortion in the two Fe^{3+} ions and noticeable values of E .

When we replace one Mn ion at the site δ by Fe, with the spin configuration shown in Fig. 2(a), we obtain an optimized total moment of $21\mu_B$. The experiment on the SMM $(\text{PPh}_4)\text{Mn}_{12}$ suggested that the ground state has a spin of $S = 19/2$.²³ We thus consider a few spin configurations with $M_s = 19/2$ that might have lower energies than that for the considered configuration with $M_s = 21/2$. A good candidate for this is obtained by

flipping only two spins coupled by J_1 from the starting spin configuration. We find that the configuration with $M_s = 19/2$ has higher energy than the $M_s = 21/2$. So the ground state has a total moment of $21\mu_B$. The ground state has the energy gap between the majority HOMO and the minority (majority) LUMO of 0.043 eV (0.424 eV). The total MAB is 41 K and $E = 0.03$ K. The magnetic easy axis is tilted by 10.7° from the z axis.

IV. DFT CALCULATIONS: POTASSIUM ADDITION

Adding electron donors such as K to the Mn_{12} molecule, we consider the following two choices for the positions of the donors. One is to place the donors at the centers of mass of the acetic acid solvent molecules in the Mn_{12} (Fig. 4). In this case, the donors are closer to the site β than the site δ by 0.92 Å. The other is to place the donors close to the favorable site δ in the x - y plane (Fig. 5). In our calculations, we use the former (latter) choice for four (two and one) K addition. If K atoms were too far away from the Mn_{12} molecule, then the unpaired electrons of the K atoms would not be transferred to the Mn_{12} molecule. The optimum distance between the K atoms and the Mn_{12} molecule is found by relaxation of the geometry. When two K atoms are added, for direct comparison with experiment,²⁴ we consider the twofold symmetric Mn_{12} molecule (Fig. 5) as well as the S_4 symmetric Mn_{12} molecule. The twofold symmetric Mn_{12} geometry is obtained from the S_4 symmetric Mn_{12} molecule by exchanging formates (HCOO) with neighboring water molecules in a twofold symmetric fashion (Fig. 5). All K added geometries we considered are charge neutral. We use a fine integration mesh and full basis sets for all atoms except for K atoms. We present results for four-, two-, and one-extra electrons added to the Mn_{12} molecule.

A. Four K addition: K_4Mn_{12}

Four K atoms are added to the Mn_{12} molecule in a S_4 symmetric fashion shown in Fig. 4). To compare with the experimental result, similarly to the four-Fe substituted geometry, we consider the three different spin configurations given in Table VII with three different magnetic moments ($M_s = 2, 4, 12$). The three considered configurations are speculated lowest-energy states for a particular M_s . We find that the configuration with $M_s = 12$ provides the lowest energy among the three (Table VII). In contrast to the Fe substitution,

when four K atoms are added, the high-spin state with $S = 12$ is the ground state. Plausible causes for this difference will be discussed later in this section and Sec. V. For the ground state, the local moments of the three sites (α , β , and δ) captured within a sphere of 2.23 Bohr radius are $-2.56 \mu_B$, $3.79 \mu_B$, and $4.16 \mu_B$, respectively. Comparing these with the local moments for the Mn_{12} geometry (Table VII vs Table I) confirms that the spin density of the extra electrons are transferred from the K atoms to primarily the site δ in the Mn_{12} molecule even though the site β is closer to the K cation than the site δ . This is in accord with the calculated projected density of $\text{Mn}(3d)$ orbitals (Fig. 3). As specified in Table VII, the local moment of the site β for the $M_s = 12$ state is $0.3 \mu_B$ higher than those for the $M_s = 2$ and $M_s = 4$ states. This indicates that for the $M_s = 12$ state the spin density of the extra electrons is not entirely localized at the site δ but there is some leakage to the site β . This may contribute to the different ground state from the Mn_8Fe_4 geometry.

We discuss the electronic and magnetic properties of the ground state. The energy gap for the majority HOMO and the minority (majority) LUMO is 1.04 eV (0.62 eV). See Table VIII. The calculated total MAB is 24 K. The projected MAB for the site δ is calculated to be 0.71 K and the easy axis of the Mn ion at the site is 51.1° tilted away from the z axis, which is qualitatively different from the projected MAB and the easy axis for the same site in the Mn_{12} geometry. See Table IV. This verifies that the absence of a Jahn-Teller instability at the site δ reduces the total MAB down to 24 K. This is only 44% of the total (2nd-order) MAB for the Mn_{12} . We notice that the projected MAB of the site β is almost half of that of the same site for the Mn_{12} or Mn_8Fe_4 geometry. This might be attributed to incomplete localization of the spin density at the site δ .

B. Double and single K additions: K_2Mn_{12} and KMn_{12}

We first consider the case that two K atoms are located close to the site δ where two water molecules are bonded in a twofold symmetric Mn_{12} molecule. The geometry is referred to as $\text{K}_2\text{Mn}_{12}(\text{trans})^*$. The optimized total moment is found to be $22 \mu_B$. Similarly to the double-Fe substituted geometry, we find that the lowest-energy of the $M_s = 10$ configurations is higher than that for the considered $M_s = 11$ configuration as shown in Table IX. So the ground state has a total spin of $S = 11$. The captured local moments on the Mn ions at the site δ are found to be $-4.15 \mu_B$ within a sphere of 2.23 Bohr radius, while those of the rest

of Mn ions do not change much compared to those for the ordinary Mn_{12} . The energy gap between the majority HOMO and the minority (majority) LUMO is 0.74 eV (0.31 eV). The calculated MAB is 31 K and $E = 0.087$ K (Table VIII).

Now we examine the case when two K atoms are added close to the sites δ in the x - y plane to the S_4 symmetric Mn_{12} . As in the case of the $\text{Mn}_{10}\text{Fe}_2$ geometry, this molecule also has *trans* and *cis* geometries. For the *cis*, however, the HOMO-LUMO energy gaps do not open up upon geometry relaxation. Thus we consider the *trans* geometry only. The energy gap between the majority HOMO and the minority (majority) LUMO is 0.82 K (0.29 K). The calculated MAB is 34 K and $E = 0.076$ K. In comparison with the $\text{K}_2\text{Mn}_{12}(\text{trans})^*$, the HOMO-LUMO energy gaps, the total MAB, and the E values agree with each other.

When only one K is added close to the site δ in the x - y plane, the optimized total moment is $21 \mu_B$. Similarly to the single-Fe-substitution case, we find that the lowest-energy state with $M_s = 19/2$ has higher energy than the considered configuration with $M_s = 21/2$. So the ground state has a total spin of $S = 21/2$ (Table IX). The ground state has an energy gap between the majority HOMO and the minority (majority) LUMO of 0.47 eV (0.036 eV). The calculated MAB is 46 K and $E = 0.033$ K. The magnetic easy axis is tilted by 4.1° from the z axis (Table VIII).

V. DISCUSSION

When several Fe ions were substituted for Mn ions at the most favorable δ sites in the Mn_{12} geometry, we found that the total spin changes as a function of the number of substituted Fe ions (extra electrons) (See Table III). The change of the total spin was the most drastic for the case of four Fe substitution. For the Mn_{12} , Mn_{11}Fe , and $\text{Mn}_{10}\text{Fe}_2$ geometries, the antiferromagnetic exchange interactions between the sites β and δ (J_4 and J'_4) are much smaller than J_1 and J_2 [Fig. 2(b)]. So the ground state has a high spin. Meanwhile, for the Mn_8Fe_4 geometry, the values of J_4 and J'_4 are large enough to flip the spins of the inner Mn ions and the spins of the Fe ions in comparison to the spin configuration of the Mn_{12} [Fig. 2(a)]. This leads to a ground state of a low spin. Although it is certain that the ground state must have a low spin, to determine the relative ordering of the $S = 2$ and $S = 4$ states, we need to rely on exact diagonalization of the Heisenberg exchange Hamiltonian. The ground state may be a noncollinear quantum state (a linear combination

of Slater determinants).

The MAB decreases with increasing number of extra electrons as shown in Fig. 6 because substituted Fe ions do not contribute to the total MAB due to a lack of Jahn-Teller distortion. Based on rigid band and intuitive argument, it was expected that the four Fe substitution would reduce the MAB more significantly than the MAB for two Fe substitution. This, however, was not found in our calculations. Although the reason is not entirely understood, it may be related to the result that the MAB varies up to a factor of 2 depending on the spin configurations given a particular geometry (Table II). This tendency has not been observed for the Mn_{12} and the Mn_4 monomer where different spin configurations gave almost the same MAB as that for the ground state.^{20,34} The major difference between the two cases is that for Mn_{12} the spin flip energies are small compared to single-electron excitations, while for the Mn_8Fe_4 the spin flip energies are comparable or higher than the single-electron excitation energy. To further understand this large deviation, we calculate the projected MABs of the sites α , β , and γ for the Mn_8Fe_4 geometry with two different spin configurations ($M_s = 4$ and $M_s = 12$). We found that the projected MAB of the site α for $M_s = 4$ is smaller than that for $M_s = 12$ and that the local easy axis of the same site for $M_s = 4$ is not as close to the x - y plane as for the case of $M_s = 12$ (Table IV). Since the projected MAB for the site α counteracts the total barrier or the projected MABs for the sites β and δ , a smaller barrier of this site would probably lead to a larger total barrier.

To investigate the relationship¹¹ between the values of E for the single- and double-Fe substituted geometries (*cis* and *trans*), we use the spin Hamiltonian [Eq. (1)] for the Mn_{12} and Mn_{11}Fe and symmetry. Suppose that the spin Hamiltonians for the Mn_{12} and Mn_{11}Fe are

$$\mathcal{H}[\text{Mn}_{12}] \equiv \sum_{\mu,\nu=x,y,z} \gamma_{\mu\nu}^{(0)} S_\mu S_\nu, \quad \mathcal{H}[\text{Mn}_{11}\text{Fe}] \equiv \sum_{\mu,\nu=x,y,z} \gamma_{\mu\nu}^{(1)} S_\mu S_\nu, \quad (3)$$

where diagonalization of the matrices $\gamma^{(0)}$ ($\gamma^{(1)}$) would provide the values of D and E . Then the spin Hamiltonian for the double-Fe substituted geometry is written, in terms of $\mathcal{H}[\text{Mn}_{12}]$ and $\mathcal{H}[\text{Mn}_{11}\text{Fe}]$, as

$$\mathcal{H}[\text{Mn}_{10}\text{Fe}_2] = \sum_{\mu,\nu=x,y,z} \gamma_{\mu\nu}^{(1)} [S_\mu S_\nu + R(S_\mu)R(S_\nu)] - \sum_{\mu,\nu=x,y,z} \gamma_{\mu\nu}^{(0)} S_\mu S_\nu \quad (4)$$

$$\equiv \sum_{\mu,\nu=x,y,z} \gamma_{\mu\nu}^{(2t),(2c)} S_\mu S_\nu \quad (5)$$

$$\gamma_{xy}^{(2t)} = 2\gamma_{xy}^{(1)}, \quad \gamma_{xz}^{(2t)} = 0, \quad \gamma_{yz}^{(2t)} = 0, \quad (6)$$

$$\gamma_{xy}^{(2c)} = 0, \quad \gamma_{xz}^{(2c)} = \gamma_{xz}^{(1)} - \gamma_{yz}^{(1)}, \quad \gamma_{yz}^{(2c)} = \gamma_{xz}^{(1)} + \gamma_{yz}^{(1)} \quad (7)$$

where R represents a proper symmetry operation and $\gamma^{(2t)}$ and $\gamma^{(2c)}$ stand for the magnetic anisotropy matrices for the *trans* and *cis* geometries, respectively. Here the magnetic anisotropy matrix γ can be calculated within DFT.¹⁹ Notice that a value of E may be determined by all of the off-diagonal elements of the matrix $\gamma^{(1)}$, while the tilting angle of the magnetic easy axis is influenced only by their xz and yz components. For the single-Fe substituted geometry the value of E is obtained by the xy , yz , and xz components of the matrix $\gamma^{(1)}$. The substantially larger tilting angle of the easy axis implies that the values of $\gamma_{xz}^{(1)}$ and $\gamma_{yz}^{(1)}$ are not as small as those calculated for the Mn_{12} with solvent disorder.^{10,11} For the *trans* geometry, due to symmetry, $\gamma_{xz}^{(2t)} = 0$ and $\gamma_{yz}^{(2t)} = 0$. Symmetry allows the nonzero off-diagonal element $\gamma_{xy}^{(2t)}$ to depend on $\gamma_{xy}^{(1)}$ only [Eq. (6)]. So the value of E for the *trans* geometry is not twice as large as the value of E for the single-Fe substituted geometry. For the *cis* geometry, although the value of $\gamma_{xy}^{(2c)}$ vanishes due to symmetry, there are nonzero values of $\gamma_{xz}^{(2c)}$ and $\gamma_{yz}^{(2c)}$. Since $\gamma_{xz}^{(2c)}$ and $\gamma_{yz}^{(2c)}$ are not small, the easy-axis tilting and the value of E are substantial for the *cis* geometry (Table III). The values of E calculated from the relaxed *trans* and *cis* geometries agree well with those obtained from Eqs. (6) and (7). The value of E for the *cis* is comparable to that for the *trans* or single-Fe substituted geometry, while the value of E for the $n = 2$ *cis* in the Mn_{12} with solvent disorder was an order of magnitude smaller than that for the $n = 1$ or $n = 2$ *trans*.

When several K atoms were added to the Mn_{12} geometry, we found that the magnetic structure and properties are primarily the same as those for Fe substitution except for a few points which will be described (Table VIII vs Table III). In both cases, the ground state has the same total spin for each number of extra electrons, except for four extra electrons. Unlike four Fe substitution, the four-K added geometry has the ground state of a high spin, $S = 12$. Similar to the case for Fe substitution, the MAB decreases with increasing number of added K atoms. Except for four-extra electrons, the K added geometries have the similar MABs to the Fe substituted geometries. The relationship between the values of E for the single- and double-Fe substituted geometries also holds for the single- and double-K added geometries. The values of E and the tilting angles of the easy axes are quite different for the two cases. We speculate that the difference between the two cases arises from incomplete localization of the spin density of the extra electrons on the sites δ for K addition. Another

difference is that when one- or two-extra electrons are added, for K addition the energy gap between the majority HOMO and minority LUMO is an order of magnitude larger than that for Fe substitution. The calculated total MAB and the local easy axis for the sites δ for both the single-K added and single-Fe substituted geometries, suggest that the geometries for one-extra electron have features in accord with the experimentally observed fast-relaxing species in a variety of low-symmetry SMMs Mn_{12} .^{36,37,38,39,40}

Although the case of the three-extra electrons was not considered in our DFT calculations, it is possible to calculate the values of D and E using the matrices $\gamma^{(0)}$ and $\gamma^{(1)}$ [Eq. (3)] and symmetry. It is found that for triple-Fe substitution $D = -0.20$ K and $E = 0.016$ K, while for triple-K addition $D = -0.29$ K and $E = 0.032$ K (Tables III and VIII). For completeness, the values of D and E for the K_2Mn_{12} (*cis*) is also calculated using Eq. (3) and symmetry: $D = -0.38$ K and $E = 0.003$ K. The value of E for the K_2Mn_{12} (*cis*) is an order of magnitude smaller than that for the $\text{Mn}_{10}\text{Fe}_2$ (*cis*). In the event that such a system is experimentally realized, the calculated values of D and E can be compared to experiment.

VI. CONCLUSION

To examine the effect of extra electrons on the electronic and magnetic structure and the magnetic anisotropy, we considered, within DFT, two classes of molecules with extra electrons in the ordinary Mn_{12} geometry: Fe substitution for Mn and K addition as electron donors. Four Fe substitution implied that the sites δ are energetically favorable for Fe ions, which agreed with experiment. Our calculations showed that the MAB decreases with increasing number of extra electrons, which is caused by absence of Jahn-Teller distortion at the sites where the extra electrons are localized. This tendency agreed with experiment and was confirmed by the calculated projected anisotropy on the sites. The total spin increases with number of extra electrons, except that the Mn_8Fe_4 geometry has the low-spin ground state due to the enhanced exchange interactions between the Fe and outer Mn ions. The S_4 symmetry-breaking geometries such as the one- and two-extra electron geometries have E values that are at least by a factor of 3 larger than those associated solvent disorder. These larger E values will significantly expedite the tunneling and eventually reduce the total MAB. Additionally, the tilting angles of the easy axes are an order of magnitude larger than those for the Mn_{12} with solvent disorder, which will provide large internal transverse

fields that will further expedite tunneling.

Acknowledgments

The authors are grateful to D. N. Hendrickson, E. M. Rumberger, and H.-L. Tsai for providing information on the published experiment on $[\text{Mn}_8\text{Fe}_4\text{O}_{12}(\text{O}_2\text{CCH}_3)_{16}(\text{H}_2\text{O})_4]$. The authors were supported in part by ONR and the DoD HPC CHSSI program.

* Electronic address: park@dave.nrl.navy.mil

† Electronic address: pederson@dave.nrl.navy.mil

- ¹ R. Sessoli, D. Gatteschi, A. Caneschi, and M.A. Novak, *Nature* (London) **365**, 141 (1993).
- ² J. R. Friedman, M. P. Sarachik, J. Tejada, and R. Ziolo, *Phys. Rev. Lett.* **76**, 3830 (1996)
- ³ E. M. Chudnovsky and J. Tejada, *Macroscopic Quantum Tunneling of the Magnetic Moment*, Cambridge Studies in Magnetism Vol. 4 (Cambridge University Press, Cambridge, 1998).
- ⁴ C. Paulsen, J. G. Park, B. Barbara, R. Sessoli, and A. Caneschi, *J. Magn. Magn. Mat.* **140**, 379 (1995).
- ⁵ T. Lis, *Acta Crystallogr. B* **36**, 2042 (1980).
- ⁶ A. L. Barra, D. Gatteschi, and R. Sessoli, *Phys. Rev. B* **56**, 8192 (1997).
- ⁷ S. Hill, J. A. A. J. Perenboom, N. S. Dalal, T. Hathaway, T. Stalcup, and J. S. Brooks, *Phys. Rev. Lett.* **80**, 2453 (1998).
- ⁸ S. Hill, S. Maccagnano, K. Park, R. M. Achey, J. M. North, and N. S. Dalal, *Phys. Rev. B* **65**, 224410 (2002).
- ⁹ E. M. Chudnovsky and D. A. Garanin, *Phys. Rev. Lett.* **87**, 187203 (2001); *Phys. Rev. B* **65**, 094423 (2002).
- ¹⁰ A. Cornia, R. Sessoli, L. Sorace, D. Gatteschi, A. L. Barra, and C. Daignebonne, *Phys. Rev. Lett.* **89**, 257201 (2002).
- ¹¹ K. Park, T. Baruah, N. Bernstein, and M. R. Pederson, *Phys. Rev. B* **69**, 144426 (2004).
- ¹² M. R. Pederson, N. Bernstein and J. Kortus, *Phys. Rev. Lett.* **89** 097202 (2002).
- ¹³ E. del Barco, A. D. Kent, E. M. Rumberger, D. N. Hendrickson, and G. Christou, *Phys. Rev. Lett.* **91**, 047203 (2003).

- ¹⁴ S. Hill, R. S. Edwards, S. I. Jones, N. S. Dalal, and J. M. North, Phys. Rev. Lett. **90**, 217204 (2003).
- ¹⁵ Considering the natural abundances of the isotopes of H, C, O, and Mn atoms, we find that 37% of Mn₁₂ molecules in a single crystal may have one or two isotopes.
- ¹⁶ E. del Barco, A. D. Kent, N. E. Chakov, L. N. Zakharov, A. L. Rheingold, D. N. Hendrickson, and G. Christou, Phys. Rev. B **69** 020411(R) (2004).
- ¹⁷ K. Park, N. S. Dalal, P. A. Rikvold, J. Chem. Phys. **117**, 11292 (2002).
- ¹⁸ T. Goto, T. Koshiba, T. Kubo, and K. Awaga, Phys. Rev. B **67**, 104408 (2003).
- ¹⁹ M. R. Pederson and S. N. Khanna, Phys. Rev. B **60**, 9566 (1999).
- ²⁰ K. Park, M. R. Pederson, and C. S. Hellberg, Phys. Rev. B **69**, 014416 (2004).
- ²¹ N. Regnault, Th. Jolicoeur, R. Sessoli, D. Gatteschi, and M. Verdaguer, Phys. Rev. B **66**, 054409 (2002).
- ²² A. R. Schake, H.-L. Tsai, R. J. Webb, K. Folting, G. Christou, and D. N. Hendrickson, Inorg. Chem. **33**, 6020 (1994).
- ²³ H. J. Eppley, H.-L. Tsai, N. de Vries, K. Folting, G. Christou, and D. N. Hendrickson, J. Am. Chem. Soc. **117**, 301 (1995).
- ²⁴ M. Soler, W. Wernsdorfer, K. A. Abboud, J. C. Huffman, E. R. Davidson, D. N. Hendrickson, and G. Christou, J. Am. Chem. Soc. **125**, 3576 (2003).
- ²⁵ W. Kohn and L. J. Sham, Phys. Rev. **140**, A1133 (1965).
- ²⁶ M. R. Pederson and K. A. Jackson, Phys. Rev. B **41**, 7453 (1990); K. A. Jackson and M. R. Pederson, *ibid.* **42**, 3276 (1990); D. V. Porezag, Ph.D. thesis, Chemnitz Technical Institute, 1997.
- ²⁷ J. P. Perdew, K. Burke, and M. Ernzerhof, Phys. Rev. Lett. **77**, 3865 (1996).
- ²⁸ D. Porezag and M. R. Pederson, Phys. Rev. A **60**, 2840 (1999).
- ²⁹ J. M. North, D. Zipse, N. S. Dalal, E. S. Choi, E. Jöblich, J. S. Brooks, and D. L. Eaton, Phys. Rev. B **67**, 174407 (2003).
- ³⁰ P. Fazekas, *Lecture Notes on Electron Correlation and Magnetism*, Series in Modern Condensed Matter Physics, (World Scientific, Singapore 1999), Vol. 5.
- ³¹ C.-I. Yang, S.-F. Yang, C.-S. Wur, G.-H. Lee, and H.-L. Tsai (unpublished).
- ³² T. Baruah and M. R. Pederson, Chem. Phys. Lett. **360**, 144 (2002).
- ³³ J. Kortus, C. S. Hellberg, and M. R. Pederson, Phys. Rev. Lett. **86**, 3400 (2001).

- ³⁴ K. Park, M. R. Pederson, and N. Bernstein, *J. Phys. Chem. Sol.* **65**, 805 (2004).
- ³⁵ In the previous calculations²⁰ of the exchange constants for the Mn₁₂, we used small basis sets for all atoms and four different exchange constants. More recently we have found that the basis sets do not affect the calculated exchange constants (unpublished).
- ³⁶ W. Wernsdorfer, R. Sessoli, and D. Gatteschi, *Europhys. Lett.* **47**, 254 (1999).
- ³⁷ Z. Sun, D. Ruiz, N. R. Dilley, M. Soler, J. Ribas, K. Folting, M. B. Maple, G. Christou, and D. N. Hendrickson, *Chem. Commun.* 1973 (1999).
- ³⁸ S. M. J. Aubin, Z. Sun, H. J. Eppley, E. M. Rumberger, I. A. Gunzei, K. Folting, P. K. Gantzel, A. L. Rheingold, G. Christou, and D. N. Hendrickson, *Inorg. Chem.* **40**, 2127 (2001).
- ³⁹ K. Takeda, K. Awaga, T. Inabe, A. Yamaguchi, H. Ishimoto, T. Tomita, H. Mitamura, T. Goto, and H. Nojiri, *Phys. Rev. B* **65**, 094424 (2002).
- ⁴⁰ Y. Suzuki, K. Takeda, and K. Awaga, *Phys. Rev. B* **67**, 132402 (2003).

TABLE I: Total fixed moments ($2M_s$), calculated local moments (sphere radii of 2.23 Bohr) associated with the three metal sites (α , β , and δ shown in Fig. 1), μ_α , μ_β , and μ_δ , energy differences from the geometry δ with $M_s = 12$, ΔE , and whether the Fermi filling is satisfied, for the ordinary Mn_{12} geometry and for the three initial tetra-Fe substituted geometries (α , β , and δ), $[\text{Mn}_8\text{Fe}_4\text{O}_{12}(\text{HCOO})_{16}(\text{H}_2\text{O})_4]$, with the spin configuration of Fig. 2(a). In the geometries α , β , and δ , four Fe ions are located at the four sites β , δ , and α shown in Fig. 1, respectively. For example, Fig. 1 shows the geometry δ .

	Mn_{12}	α	β	δ	α	β	δ
M_s	10	12	12	12	11	11	11
μ_α	-2.58	-1.55	-2.59	-2.54	-1.84	-2.59	-2.57
μ_β	3.62	3.60	3.94	3.59	3.51	3.74	3.45
μ_δ	3.55	3.52	3.64	3.95	3.48	3.55	3.83
ΔE (eV)		1.119	1.186	0	1.826	1.106	0.157
Fermi filling	Yes	Yes	No	Yes	No	Yes	No

TABLE II: Total moments ($2M_s$), down spins (the rest of spins are in an up state and each spin is numbered following Fig. 2(b)), Ising energy expressions [Eq. (2)], the energy differences from the lowest-energy spin configuration ($M_s = 4$) ΔE , the MABs for the fourteen collinear spin configurations in the tetra-Fe substituted geometry shown in Fig. 1. Here $M_s = 2$ (V-2) denotes a spin configuration with $M_s = 2$ which is different from the other three configurations with $M_s = 2$. The exchange coupling constants J_1, J_2, J_3, J'_3, J_4 , and J'_4 , are defined in Fig. 2(b).

M_s	down spins	Ising energy	ΔE (eV)	MAB (K)
2	2,4,5,6,7,8	$E_0 - 9J_3 + 4.5J'_3 - 20J_4 - 20J'_4$	0.2764	26
2 (II)	1,3,4,6,8,10	$E_0 - 6J_1 - 15J_2 - 10J_4 + 10J'_4$	0.4016	
2 (IV)	1,8,9,10,11	$E_0 - 15J_2 - 20J'_4$	0.2747	29
2 (V-2)	5,6,7,11,12	$E_0 - 6J_1 + 9J_3 + 4.5J'_3 - 10J_4 - 10J'_4$	0.3941	22
4	9,10,11,12	$E_0 + 12J_1 - 30J_2 + 9J_3 + 4.5J'_3 - 20J_4 - 20J'_4$	0	33
4 (I)	1,2,3,4,6,8	$E_0 - 30J_2 + 9J_3 + 4.5J'_3$	0.2808	22
4 (II-1)	1,3,6,11,12	$E_0 - 6J_1 - 9J_3 + 4.5J'_3 - 10J_4 - 10J'_4$	0.4131	21
4 (II-2)	2,3,6,11,12	$E_0 + 6J_1 - 15J_2 - 4.5J'_3 - 10J_4 - 10J'_4$	0.3262	27
4 (III)	1,6,7,8,12	$E_0 - 12J_1 + 15J_2 - 20J_4$	0.5265	16
5	8,9,10,11	$E_0 + 6J_1 - 15J_2 + 9J_3 + 4.5J'_3 - 20J'_4$	0.3312	32
6	1,10,11,12	$E_0 + 6J_1 - 15J_2 - 10J_4 - 10J'_4$	0.3407	27
7	1,2,4,7,8	$E_0 - 6J_1 - 15J_2$	0.4240	22
8	5,6,7,8	$E_0 - 12J_1 + 30J_2 + 9J_3 + 4.5J'_3 - 20J_4 - 20J'_4$	0.5334	24
12	1,2,3,4	$E_0 - 12J_1 - 30J_2 + 9J_3 + 4.5J'_3 + 20J_4 + 20J'_4$	0.6013	19

TABLE III: Calculated total spins, the second-order magnetic anisotropy parameters (D and E), easy-axis tilting angles θ (angles between the local easy axes and the z axis), MABs, the energy gaps between majority HOMO and minority (majority) LUMO for the Mn_{12} and the Fe substituted geometries. Except for Mn_9Fe_3 the lowest-energy spin configuration has been used for each geometry. For Mn_9Fe_3 results are determined from Eq. (3) and the use of symmetry.

	Mn_{12}	Mn_{11}Fe	$\text{Mn}_{10}\text{Fe}_2(\text{trans})$	$\text{Mn}_{10}\text{Fe}_2(\text{cis})$	Mn_9Fe_3	Mn_8Fe_4
S	10	21/2	11	11		4
D (K)	-0.54	-0.42	-0.29	-0.33	-0.20	-2.10
E (K)	0.0	0.030	0.045	0.020	0.016	0.0
θ (deg)	0.0	10.7	0.0	19.0		0.0
MAB (K)	54	41	31	33		33
maj H - min L (eV)	0.804	0.043	0.075	0.030		0.664
maj H - maj L (eV)	0.438	0.424	0.432	0.427		0.247

TABLE IV: Calculated projected (local) MABs Δ_i and tilting angles of the local easy axes φ_i for the sites, α , β , and δ (Fig. 1), in the Mn_{12} ($S = 10$), Mn_8Fe_4 ($S = 4$), Mn_8Fe_4 ($S = 12$), $\text{Mn}_{10}\text{Fe}_2$ ($S = 11$), and K_4Mn_{12} ($S = 12$) geometries.

	$\text{Mn}_{12}(S = 10)$	$\text{Mn}_8\text{Fe}_4 (S = 4)$	$\text{Mn}_8\text{Fe}_4 (S = 12)$	$\text{Mn}_{10}\text{Fe}_2 (S = 11)$	$\text{K}_4\text{Mn}_{12} (S = 12)$
Δ_α (K)	0.87	0.21	0.96	1.16	0.85
Δ_β (K)	9.7	9.5	9.8	10.4	5.5
Δ_δ (K)	9.3	0.82	0.41	0.95	0.71
φ_α (degree)	83.8	58.9	87	83	83.4
φ_β (degree)	9.8	8.5	8.3	9.4	9.1
φ_δ (degree)	36.2	65.8	61.5	63	51.1

TABLE V: DFT-determined and experimental exchange constants for the tetra-Fe substituted geometry shown in Fig. 1 and the Mn_{12} geometry. In this study, a fine mesh and full basis sets were used for both the Mn_8Fe_4 and Mn_{12} geometries. For the Mn_8Fe_4 , the fourteen spin configurations were used (Table II), while for the Mn_{12} , the eleven spin configurations were used (Ref.[20]). For comparison with other published results, a DFT-determined value of J_3 (J_4) represents an average between the values of J_3 and J'_3 (J_4 and J'_4) shown in Fig. 2(b). The exchange constants for the Mn_{12} shown here are slightly different from those reported in Ref. [20] because in the previous study smaller basis sets and fewer exchange constants were used ($J_3 = J'_3$ and $J_4 = J'_4$).

	Mn_8Fe_4 (DFT)	Mn_8Fe_4 (Exp[Ref. 22])	Mn_{12} (DFT)	Mn_{12} (Exp[Ref. 21])
S	4	2	10	10
J_1	119	432	140	119
J_2	150	397	117	118
J_3	7.2	173	7.2	-8
J_4	122	187	24	23

TABLE VI: Total moments ($2M_s$), down spins, the energy differences from the $M_s = 21/2$ ($M_s = 11$) geometry, and whether Fermi filling is satisfied, for the different spin configurations in the Mn_{11}Fe ($\text{Mn}_{10}\text{Fe}_2$ *trans*) geometry. For the Mn_{11}Fe geometry, an Fe ion occupies site 12 shown in Fig. 2(b). For the $\text{Mn}_{10}\text{Fe}_2$ geometry, two Fe ions occupy sites 9 and 11 shown in Fig. 2(b). The spin configurations for the $M_s = 21/2$ and $M_s = 11$ geometries are the same as Fig. 2(a). The configurations for the $M_s = 19/2$ and $M_s = 10$ are obtained by exchanging spin 1 with spin 5 in Fig. 2(b).

	Mn_{11}Fe		$\text{Mn}_{10}\text{Fe}_2(\textit{trans})$	
M_s	19/2	21/2	10	11
down spins	2,3,4,5	1,2,3,4	2,3,4,5	1,2,3,4
ΔE (eV)	0.035	0	0.014	0
Fermi filling	Yes	Yes	Yes	Yes

TABLE VII: Total moments ($2M_s$), down spins, local moments captured around the three sites, α , β , and δ (Fig. 1), the energy differences from the lowest-energy spin configuration, whether Fermi filling is satisfied, and MABs, for the three different spin configurations in the four-K added Mn_{12} geometry, $\text{K}_4[\text{Mn}_{12}\text{O}_{12}(\text{HCOO})_{16}(\text{H}_2\text{O})_4]$ shown in Fig. 4. For $M_s = 2$, there are two slightly different local moments because of the twofold symmetry of the spin configuration. For $M_s = 4$ and $M_s = 12$, the spin configurations are fourfold symmetric.

M_s	2	4	12
down spins	2,4,5,6,7,8	9,10,11,12	1,2,3,4
μ_α (μ_B)	2.78, 2.52	2.61	-2.56
μ_β (μ_B)	3.44, 3.48	3.49	3.79
μ_δ (μ_B)	-4.20, -4.21	-4.16	4.16
ΔE (eV)	0.576	0.359	0
Fermi filling	Yes	Yes	Yes
MAB (K)	20	32	24

TABLE VIII: Calculated total spins, the second-order magnetic anisotropy parameters, easy-axis tilting angles, the MABs, the energy gaps between majority HOMO and minority (majority) LUMO for the K added Mn_{12} geometries. For $\text{K}_2\text{Mn}_{12}(\text{cis})$ and K_3Mn_{12} results are determined from Eq. (3) and the use of symmetry.

	KMn_{12}	$\text{K}_2\text{Mn}_{12}(\text{trans})$	$\text{K}_2\text{Mn}_{12}(\text{trans})^*$	$\text{K}_2\text{Mn}_{12}(\text{cis})$	K_3Mn_{12}	K_4Mn_{12}
S	21/2	11	11			12
D (K)	-0.46	-0.36	-0.35	-0.38	-0.29	-0.16
E (K)	0.033	0.076	0.087	0.003	0.032	0.0
θ (degree)	4.1	0.0	0.0			0.0
MAB (K)	45.7	34	31			24
maj H - min L (eV)	0.47	0.82	0.74			1.04
maj H - maj L (eV)	0.036	0.29	0.31			0.62

TABLE IX: Total moments, down spins, local moments, the energy differences from the lowest-energy spin configuration, and whether Fermi filling is satisfied, for two different spin configurations in the double K- and single-K added Mn₁₂ geometries. In the *trans* geometry marked by *, the twofold symmetric Mn₁₂ geometry (Fig.5) was used.

	K[Mn ₁₂ O ₁₂]		K ₂ [Mn ₁₂ O ₁₂]* (<i>trans</i>)	
M_s	19/2	21/2	10	11
down spins	2,3,4,5	1,2,3,4	2,3,4,5	1,2,3,4
ΔE (eV)	0.0823	0	0.3225	0
Fermi filling	Yes	Yes	Yes	Yes

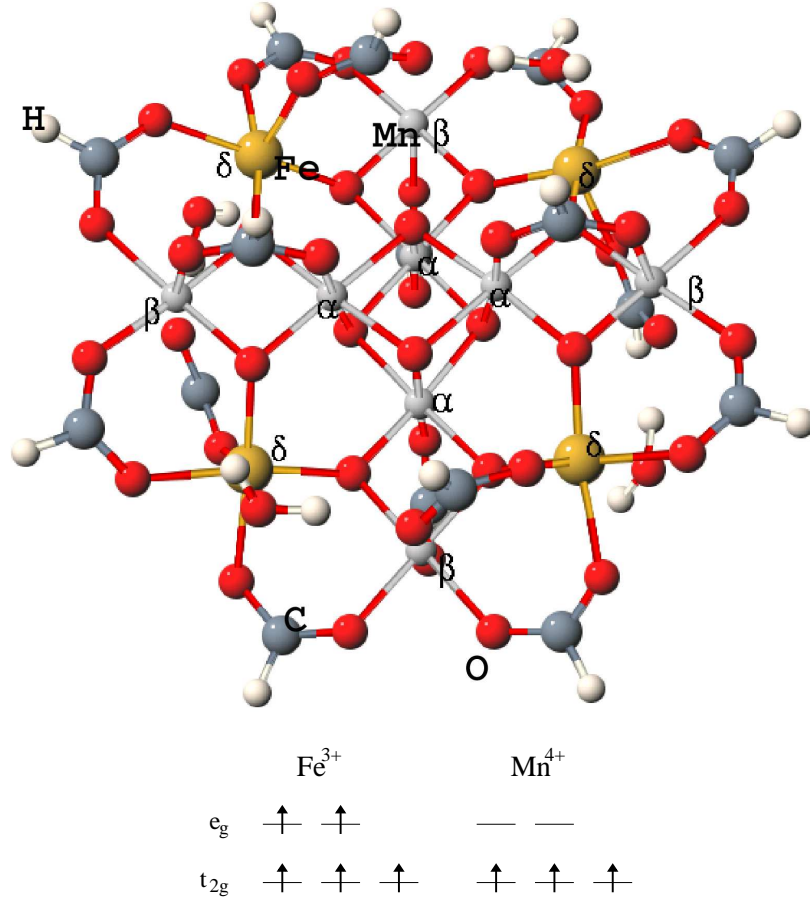


FIG. 1: Schematic diagram of the fourfold symmetric tetra-Fe substituted Mn_{12} geometry, $\text{Mn}_8\text{Fe}_4\text{O}_{12}(\text{HCOO})_{16}(\text{H}_2\text{O})_4$. The shading scheme of the atoms is as follows: darkness increases from H (white), to Mn, to Fe (largest spheres), to C, and to O (darkest). The three inequivalent metal ion sites are labeled as α , β , and δ . The bottom figures illustrate occupancy of the e_g and t_{2g} $3d$ orbitals for Fe^{3+} (or Mn^{2+}) and Mn^{4+} .

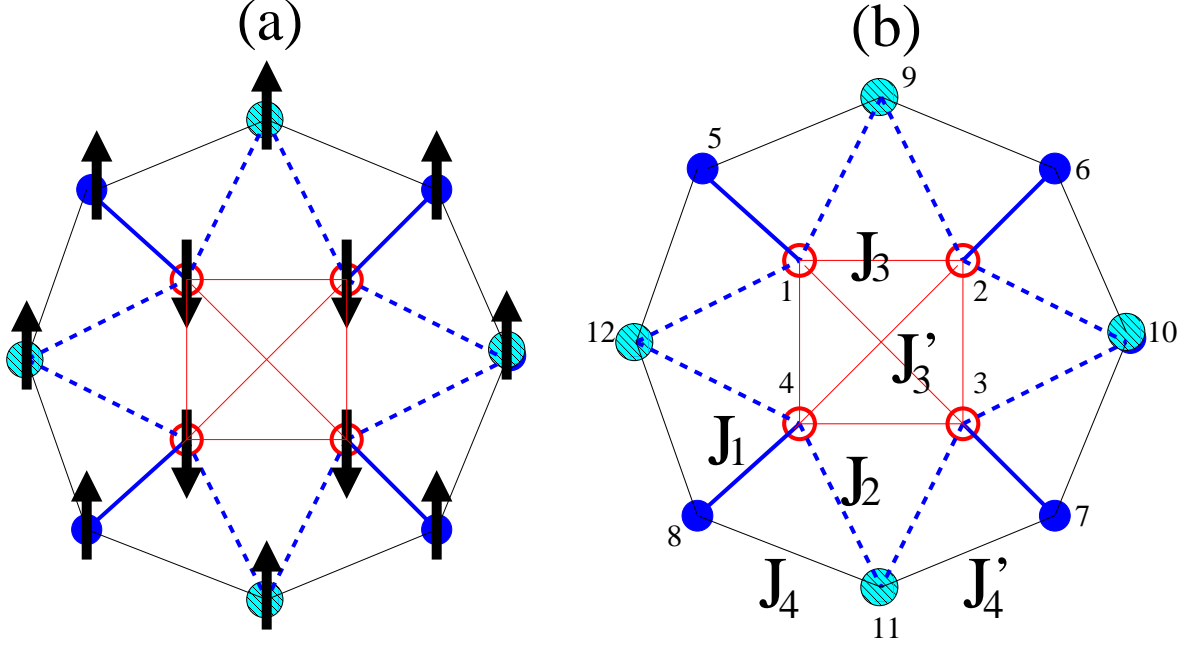


FIG. 2: (a) Initial spin configuration considered for the fourfold symmetric $\text{Mn}_8\text{Fe}_4\text{O}_{12}(\text{HCOO})_{16}(\text{H}_2\text{O})_4$ geometry to determine the most favorable sites for extra electrons. The inequivalent sites are indicated by the three different symbols. (b) Schematic diagram of the exchange constants, J_1 , J_2 , J_3 , J'_3 , J_4 , and J'_4 , where J_3 and J'_3 (J_4 and J'_4) are slightly different from each other because of a difference in the bond length by approximately 0.1\AA . Each spin is labeled from 1 to 12. The sites α correspond to spins 1-4, the sites β to spins 5-8, and the sites δ to spin 9-12.

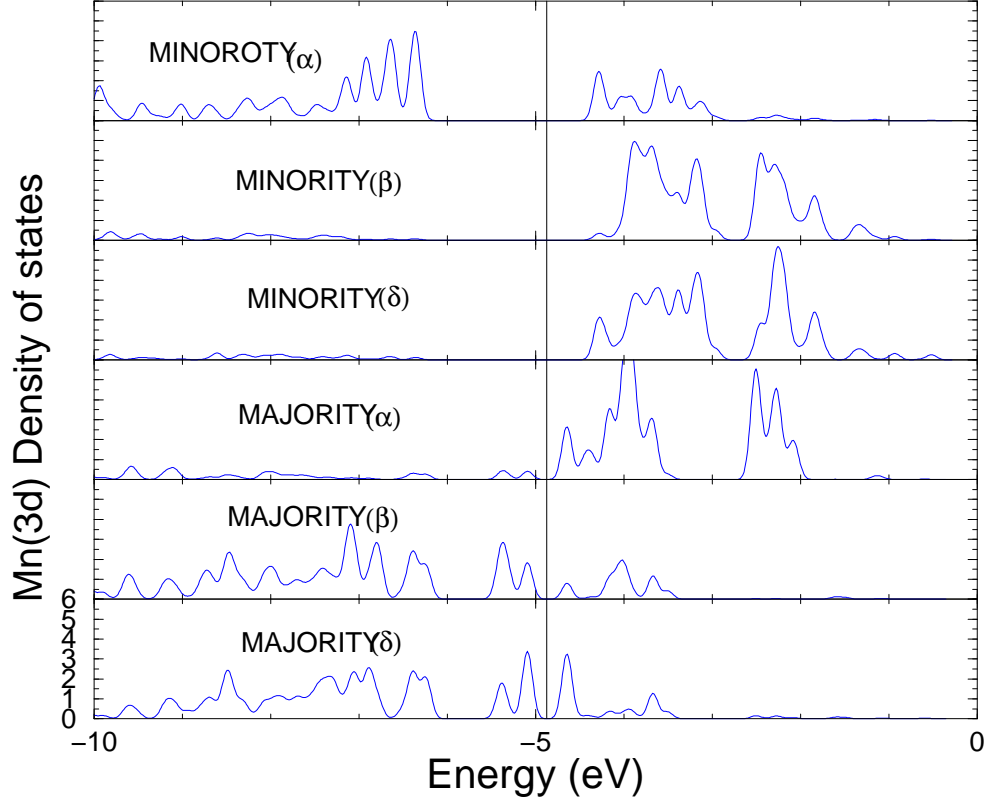


FIG. 3: Calculated density of states projected onto the majority and minority Mn(3d) orbitals at each of the three inequivalent sites (α , β , and δ) for the fourfold symmetric $[\text{Mn}_{12}\text{O}_{12}(\text{HCOO})_{16}(\text{H}_2\text{O})_4]$ whose structure is exactly the same as Fig. 1 with Fe replaced by Mn. The solid vertical line denotes the Fermi energy level.

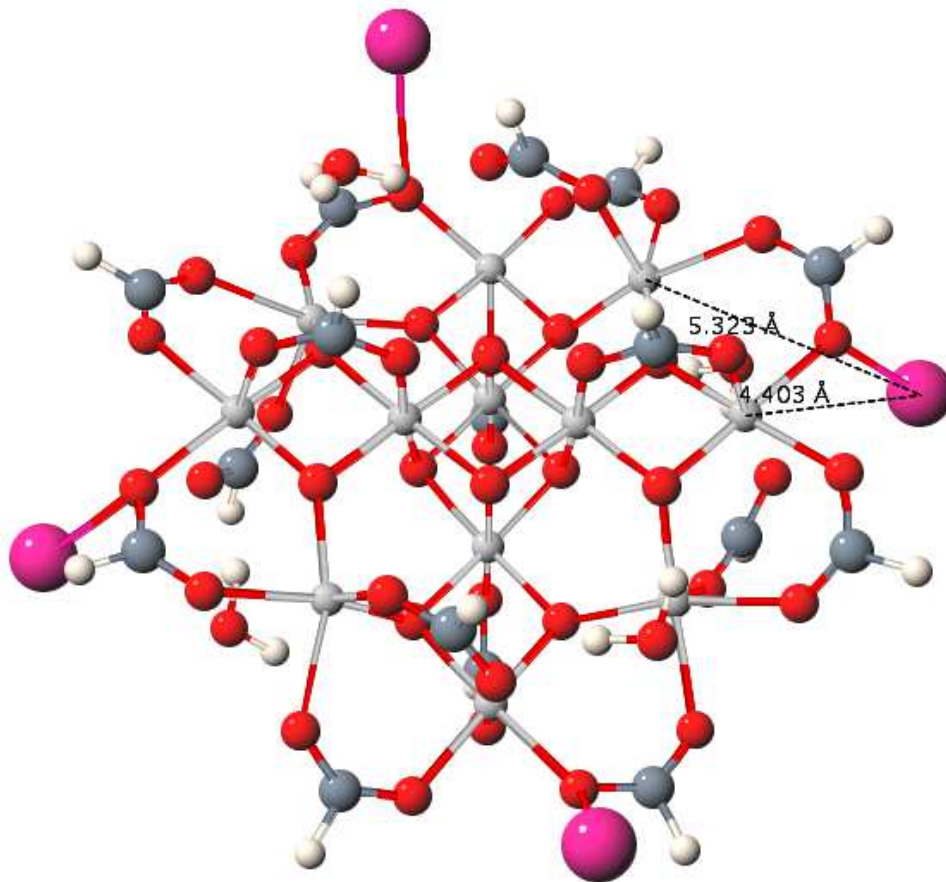


FIG. 4: Schematic diagram of the fourfold symmetric $\text{K}_4[\text{Mn}_{12}\text{O}_{12}(\text{HCOO})_{16}(\text{H}_2\text{O})_4]$ geometry, where two of the K cations are located slightly above the x - y plane and the rest two are slightly below the x - y plane. The shading scheme is the same as that for Fig. 1 except that the largest spheres are now K cations. The distance between the closest Mn β site (δ site) and K is 4.403 Å (5.323 Å).

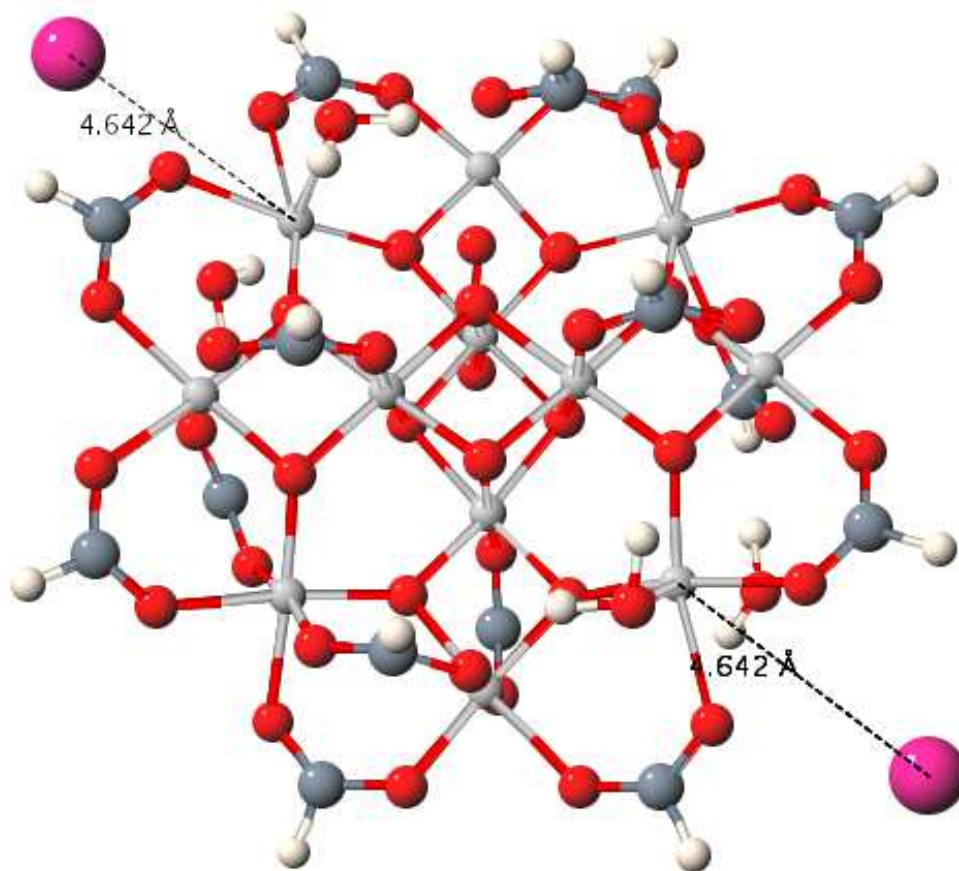


FIG. 5: Schematic diagram of the *twofold* symmetric $\text{K}_2[\text{Mn}_{12}\text{O}_{12}(\text{HCOO})_{16}(\text{H}_2\text{O})_4]$ geometry, where two K cations are close to the site δ in the x - y plane. The shading scheme is the same as that for Fig. 4. The distance between the closest Mn and K is about 4.642 Å.

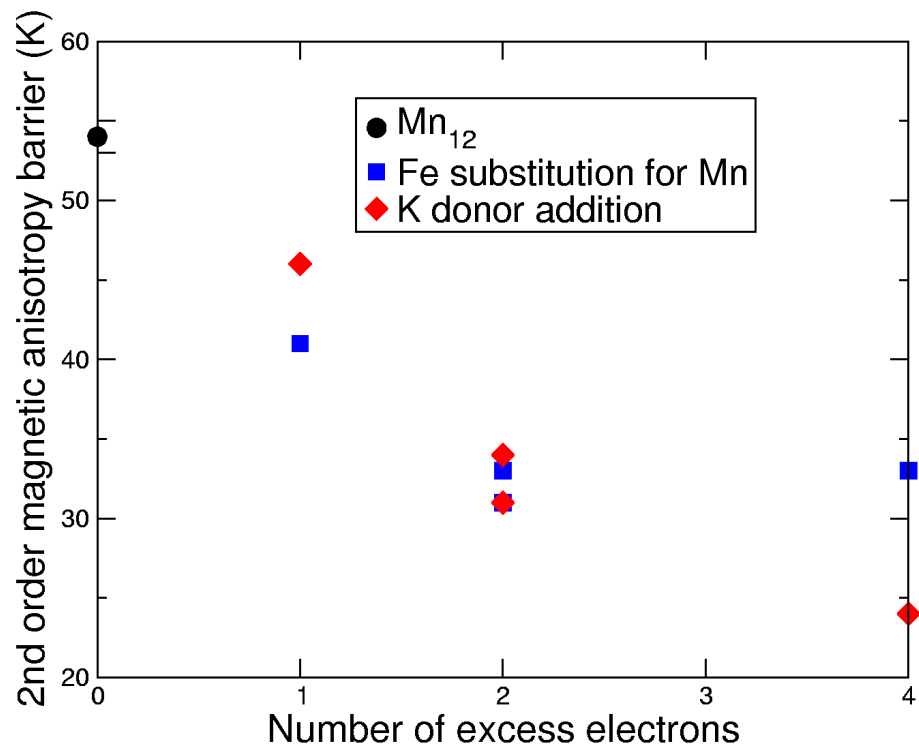


FIG. 6: Calculated MAB vs number of extra electrons for the Fe substituted and K added Mn₁₂ geometries and the Mn₁₂ geometry.